Nucleus Accumbens Fast-Spiking Interneurons Constrain Impulsive Action

Marc T. Pisansky[1], Emilia M. Lefevre[1], Cassandra L. Retzlaff[1], Brian H. Trieu[2] & Patrick E. Rothwell[1]*

[1]Department of Neuroscience, University of Minnesota - Twin Cities, Minneapolis, MN

[2]Graduate Program in Neuroscience, University of Minnesota - Twin Cities, Minneapolis, MN

*Corresponding Author:

Patrick E. Rothwell, Ph.D.
4-283 Wallin Medical Biosciences Building
2101 6th Street SE
Minneapolis, MN, 55455
Phone: 612-626-8744
Email: rothwell@umn.edu

Running title: Accumbens fast-spiking interneurons inhibit impulsivity

Keywords: impulsivity, parvalbumin, interneuron, nucleus accumbens, fiber photometry, chemogenetics

Number of words in abstract: 249

Number of figures: 6 (embedded within text)

Number of tables: 1 (embedded within text)

Supplemental information: 6 figures (located at end of document)

ABSTRACT

Background: The nucleus accumbens (NAc) controls multiple facets of impulsivity, but is a heterogeneous brain region with diverse microcircuitry. Prior literature links impulsive behavior in rodents to gamma aminobutyric acid (GABA) signaling in the NAc. Here, we studied the regulation of impulsive behavior by fast-spiking interneurons (FSIs), a strong source of GABAergic synaptic inhibition in the NAc.

Methods: Male and female transgenic mice expressing Cre recombinase in FSIs allowed us identify these sparsely distributed cells in the NAc. We used the 5-choice serial reaction time (5-CSRT) task to measure both impulsive action and sustained attention. During the 5-CSRT task, we monitored FSI activity with fiber photometry calcium imaging, and manipulated FSI activity with chemogenetics. We used electrophysiology, optogenetics, and fluorescent *in situ* hybridization to confirm these methods were robust and specific to FSIs.

Results: In mice performing the 5-CSRT task, NAc FSIs showed sustained activity on trials ending with correct responses. In contrast, FSI activity declined over time on trials ending with premature responses, as well as trials in which responses were omitted. Chemogenetic inhibition of NAc FSIs did not change response latencies or general locomotor activity, but significantly increased the number of premature responses, while the number of omission trials either remained constant or decreased.

Conclusions: These experiments provide strong evidence that NAc FSIs constrain impulsive actions, most likely by GABA-mediated synaptic inhibition of medium spiny neuron output. Our findings may provide insight into the pathophysiology of impulse control disorders, and inform the development of circuit-based therapeutic interventions.

INTRODUCTION

Impulsivity is defined as the tendency to act prematurely or without foresight, and involves a failure of cognitive control that characterizes various neuropsychiatric diseases (1, 2). Notably, impulsivity represents a vulnerability marker for substance use disorders (3), attention deficit/hyperactivity disorder (ADHD) (4, 5), and suicidality (6). The nucleus accumbens (NAc), a major hub in limbic circuits that regulate reward-seeking behavior, plays a critical role in controlling multiple facets of impulsivity (7). Evidence for this role comes from human brain imaging studies (8–11), as well as local pharmacological manipulations and brain lesion studies in rodents (12–17). These approaches have identified key neuromodulatory systems and provided critical insight into the aggregate function of the NAc, but we still have a limited understanding of how impulsive behavior is regulated by the activity of specific cell types embedded within NAc microcircuitry.

Gamma aminobutyric acid (GABA) has been implicated as a modulator of impulsivity in the NAc (18, 19) and other brain regions (20). A major source of local GABAergic signaling in these brain regions are fast-spiking interneurons (FSIs), a cell type frequently defined by parvalbumin (PV) expression (21). FSIs provide robust feed-forward inhibition that constrains and sculpts the output of projection neurons in the NAc (22–24), dorsal striatum (25–27), and other brain regions (28–30). FSIs in the prefrontal cortex regulate complex cognitive processes like attention (31), while FSIs in the dorsal striatum have been implicated in procedural learning (32) and habit formation (33). Manipulations of FSIs in the NAc alter behavioral responses to addictive drugs (34, 35), but the specific contribution of these cells to impulsivity has yet to be explored.

In this study, we investigated the function of NAc FSIs in mice performing the 5-choice serial reaction time (5-CSRT) task, a classic behavioral assay that measures sustained attention and impulse control (36). We focused on FSIs in the NAc core subregion, where GABAergic signaling has specifically been linked to impulsive behavior in this task (18). To monitor the activity of FSIs in behaving mice, we used a viral approach to express a genetically-encoded calcium indicator, and monitored fluorescent signals using *in vivo* fiber photometry. These calcium imaging experiments reveal that sustained activity of FSIs is associated with successful control of impulsive action. We then used chemogenetic methods to inhibit the activity of FSIs in the NAc core, and found this manipulation increased impulsivity. Together, our data suggest that FSIs in the NAc play an important role in constraining impulsive actions.

METHODS AND MATERIALS

Subjects

Male and female mice C57/B6J mice were housed with same-sex littermates on a 12 hr light/dark cycle, and used for experiments at 8-20 weeks of age. PV-2A-Cre transgenic mice (37) were obtained from The Jackson Laboratory (JAX stock #012358). All procedures conformed to the National Institutes of Health *Guidelines for the Care and Use of Laboratory Animals*, and were approved by the University of Minnesota Institutional Animal Care and Use Committee

5-Choice Serial Reaction Time (5-CSRT) Task

As previously described (38), mice were food-restricted to ~85% of free-feeding body weight, and pre-exposed to 14 mg purified dustless precision pellets (Bio-Serv) in the home cage. Behavioral training took place in standard mouse operant chambers (Med Associates), and began with two consecutive days of magazine training (30 food pellets delivered randomly over 30 minutes). We then began the first of eight training stages (**Table 1**), using a protocol adapted from previous studies of rats (39) and mice (40, 41). Each trial was signaled by the offset of a house light, followed by illumination of cue lights located inside five nose-poke apertures on the wall across from the food magazine. In Stage 1 of training, cues were immediately and continuously presented in all five apertures, and a response in any aperture was rewarded. In Stage 2 of training, a cue light was immediately and continuously presented in only one aperture. Correct responses in this aperture were rewarded, while incorrect responses in any other aperture were punished with illumination of the house light during a time-out period (five seconds). Mice moved on to the next stage after receiving 50 rewards before the end of each 60-minute session.

In Stage 3 and subsequent stages, each trial began with an inter-trial interval (ITI) prior to cue presentation. Mice were required to withhold responses during the ITI, and premature responses during this period were punished with a time-out. The duration of cue presentation was also limited, and failures to respond ("omissions") were punished with a time-out. Correct responses to the cued aperture were rewarded, and additional nose-pokes that followed a correct response but preceded retrieval of the reward were recorded as perseverative responses. Mice progressed to the next stage after reaching 50% accuracy, defined as the number

of correct trials over the total number of all trial types. At various stages of training in different experiments, we also conducted tests of impulsivity and attention, in which either the ITI length or cue duration varied randomly from trial to trial (2.5-20 sec) within a single session.

Training Stage	ITI Length (s)	Cue Duration (s)
1	N/A	∞ (all cues)
2	N/A	∞ (single cue)
3	2.5	20
4	5	10
5	5	8
6	5	4
7	5 – 10	4
8	5 – 10	2
Impulsivity Test	2.5, 5, 10, 20	5
Attention Test	5	2.5, 5, 10, 20

Table 1. Training protocol for the 5-CSRT task

Plasmids and Adeno-Associated Viral Vectors

pAAV-Syn-FLEX-rc[ChrimsonR-tdTomato] was a gift from Edward Boyden (Addgene plasmid #62723). pGP-AAV-CAG-FLEX-jGCaMP7s-WPRE was a gift from Douglas Kim (Addgene plasmid #104495). A Cre-inactivated (DO) version (42) of jGCaMP7s with a CaMKII promoter was cloned University of Minnesota Viral Vector and Cloning Core, which also packaged ChrimsonR and jGCaMP7s constructs in the AAVdj serotype (43). Other viral vectors were obtained from the Stanford University Gene Vector and Virus Core (AAVdj-EF1a-FLEX-eYFP) and Addgene (AAV8-hSyn-FLEX-hM4Di-mCherry; viral prep #44362-AAV8). All viral vectors were used at a concentration of $5x10^{12}$ particles/mL.

Stereotaxic Surgery

Intracranial virus injection and fiber-optic implantation were performed as previously described (38), with the following modifications. Mice were anesthetized with a ketamine:xylazine cocktail (100:10 mg/kg), and a small hole was drilled above target coordinates for the NAc core (AP +1.50, ML $\pm$1.10; DV -4.40). A 33-gauge Hamilton syringe containing viral solution was slowly lowered to these target coordinates, followed by injection

of 0.75 µL at a rate of 0.1 µL/min. The syringe tip was left in place at the injection site for 5 minutes, and then slowly retracted over the course of five minutes. For fiber photometry experiments, a 400 µm fiberoptic cannula (Doric Lenses: MFC_400/430-0.48_6mm_MF1.25_FLT) was implanted just above the site of virus injection (+0.02 mm), and fixed to the scull using a dual-cure resin (Patterson Dental, Inc.). After surgery, mice were given 500 µL saline and 5 mg/kg carprofen (s.c.) daily for three days, and recovered a minimum of 7 days before any behavioral training.

Fluorescent *in situ* Hybridization

PV-2A-Cre mice expressing AAVdj-hSyn-FLEX-ChrimsonR-tdTomato in the NAc were anesthetized with isoflurane and decapitated. Brains were rapidly frozen on dry ice in OCT embedding medium, and coronal sections (10 µm) were collected on positively charged glass slides and stored at -80°C until processing. Fluorescent *in situ* hybridization was performed using the RNAscope Multiplex Fluorescent Assay (Advanced Cell Diagnostics) according to manufacturer protocol. Briefly, the day before running the assay, slides were post-fixed in 4% PFA for 15 min at 4°C, followed by dehydration in increasing concentrations of ethanol (50%>70%>100%) for 5 min each at room temperature (RT). After the final 100% ethanol wash, slides were stored at -20°C in 100% ethanol overnight. The following day, slides were left to air dry and a hydrophobic barrier was painted around sections to be analyzed. Protease IV was applied to sections of interest for 30 min at RT, followed by two brief washes in 1x PBS. Hybridization probes for *Pthlh* (456521), *Pvalb* (421931-C2), and tdTomato (317041-C3) were applied to sections and incubated at 40°C for 2 hours, then washed twice in 1x RNAscope buffer for 2 minutes. Amplification was performed using AMP1-4 detection reagents, which were applied sequentially and incubated for 15-30 min each at 40°C, washing with 1X RNAscope wash buffer between each reagent. After the final wash, slides were shaken dry and mounting medium (Invitrogen Prolong Gold antifade reagent with DAPI) was applied before coverslips were placed on the slides. Images were taken using a Keyence BZX fluorescence microscope under a 40X objective.

Electrophysiology

PV-2A-Cre mice expressing AAV8-hSyn-FLEX-hM4Di-mCherry in the NAc were anesthetized with isoflurane and decapitated. Brains were quickly removed and placed in ice-cold cutting solution containing (in

mM): 228 sucrose, 26 $NaHCO_3$, 11 glucose, 2.5 KCl, 1 NaH_2PO_4-H_2O, 7 $MgSO_4$-$7H_20$, 0.5 $CaCl_2$-$2H_2O$. Coronal slices (240 µm thick) containing the NAc were collected using a vibratome (Leica VT1000S) and allowed to recover in a submerged holding chamber with artificial cerebrospinal fluid (aCSF) containing (in mM): 119 NaCl, 26.2 $NaHCO_3$, 2.5 KCl, 1 NaH_2PO_4-H_2O, 11 glucose, 1.3 $MgSO_4$-$7H_2O$, 2.5 $CaCl_2$-$2H_2O$. Slices recovered in warm ACSF (33°C) for 10-15 minutes and then equilibrated to room temperature for at least one hour before use. Slices were transferred to a submerged recording chamber and continuously perfused with aCSF at a rate of 2 mL/min at room temperature. All solutions were continuously oxygenated (95% O_2/5% CO_2).

Whole-cell current-clamp recordings from FSIs or MSNs were obtained under visual control using IR-DIC optics. FSIs were distinguished from putative MSNs by the presence or absence of mCherry fluorescence, respectively, using an Olympus BX51W1 microscope. Borosilicate glass electrodes (3-5 MΩ) were filled with (in mM): 120 K-Gluconate, 20 KCl, 10 HEPES, 0.2 EGTA, 2 $MgCl_2$, 4 ATP-Mg, 0.3 GTP-Na (pH 7.2-7.3). Cells were injected with a series of current steps (1 s duration) from -100 to +250 pA. For chemogenetic experiments, maximum firing rate and resting membrane potential were analyzed for each cell, before and after bath application of clozapine-N-oxide (CNO, 3 µM). Membrane potential measurements were corrected for a liquid junction potential of ~8 mV. Maximum firing rate was calculated as the average maximum firing rate over the 1 s step that could be sustained without inducing a depolarization block. Action potential (AP) half-width was measured at the half-way point between threshold and the AP peak. Recordings were performed using a MultiClamp 700B (Molecular Devices), filtered at 2 kHz, and digitized at 10 kHz. Data acquisition and analysis were performed online using Axograph software. Series resistance was monitored continuously and experiments were discarded if resistance changed by >20%.

Fiber Photometry

For fiber photometry experiments, separate groups of PV-2A-Cre mice received unilateral injection of the following virus combinations into the NAc:

AAVdj-EF1a-FLEX-eYFP (negative control group, n = 3: 1 male, 2 female)

AAVdj-hSyn-FLEX-ChrimsonR-tdTomato & AAVdj-CAG-FLEX-jGCaMP7s (n = 7: 4 male, 3 female)

AAVdj-hSyn-FLEX-ChrimsonR-tdTomato & AAVdj-CaMKII-DO-jGCaMP7s (n = 4: 2 male, 2 female)

Fiber photometry recordings were conducted a minimum of two weeks after surgery, to allow for sufficient viral expression. Recordings from mice in the 5-CSRT task were conducted after a single session of Stage 8 training. Real-time data were acquired using a RZ5P fiber photometry workstation (Tucker Davis Technologies). As previously described (44), 470 nm and 405 nm LEDs (ThorLabs, M470F3 and M405F1) were modulated at distinct carrier frequencies (531 Hz and 211 Hz, respectively), and passed through a fluorescence mini cube (Doric Lenses) coupled into a patch cord (400 µm, 0.48 NA). For experiments involving red-shifted optogenetic stimulation, a 565nm LED (ThorLabs, M595F2) was connected to the fluorescence mini cube and coupled to the same patch cord, and controlled using a pulse generator (Master-8, A.M.P.I.) The distal end of the patch cord was connected to the implanted fiberoptic cannula with a ceramic sleeve. Fluorescence was back-projected through the mini cube and focused onto a photoreceiver (Newport Model 2151, FC adapter). Signals were sampled at 6.1 kHz, demodulated in real-time, and saved for offline analysis. For the 5-CSRT task, behaviorally relevant events (including trial onset, cue onset/offset, nose poke, and magazine entry) were transmitted to the fiber photometry workstation as TTL signals from the operant chambers.

The change in fluorescent signal (dF/F) was calculated within each session as described (44). Each channel was low-passed filtered (<2Hz) and a linear least-squared model fit the isosbestic control signal (405 nm) to the calcium-dependent signal (470 nm). Change in fluorescence was calculated as ([470nm signal − fitted 405nm signal]/[fitted 405nm signal]). In most experiments, we also subtracted the eighth percentile value of dF/F over a rolling 20 second window (45), which effectively corrected for photobleaching over time. However, this correction was not applied in fiber photometry experiments validating chemogenetic inhibition of FSIs (**Supplementary Figure S3**), in order to detect slow changes in the fluorescent signal following CNO injection. For event-related analyses, normalized dF/F was computed using the mean value of a two-second window before trial onset as baseline.

Chemogenetic Manipulations of Behavior

PV-2A-Cre mice (n = 14: 10 male, 4 female) and wild-type littermates (n = 14: 7 male, 7 female) received bilateral injection of AAV8-hSyn-FLEX-hM4Di-mCherry into the NAc. After recovery, these mice were trained on the 5-CSRT through Stage 8, which provided at least four weeks of viral expression. After one day of training in Stage 8, mice received i.p. injections of either saline or 2 mg/kg CNO (Hello Bio) 30 minutes prior to testing on

Stage 8. Saline and CNO sessions were conducted on separate days in counterbalanced order. After these tests, mice completed attention and impulsivity tests, again preceded by counterbalanced i.p. injections of saline or CNO (2 mg/kg).

We tested open-field locomotor activity in this same group of animals, using an arena (ENV-510, Med Associates) housed within a sound-attenuating chamber. The location of the mouse within the arena was tracked in two dimensions by arrays of infrared beams connected to a computer running Activity Monitor software (Med Associates). All mice were acclimated to the arena for one session on the day prior to testing, and then received i.p. injection of saline or CNO (2 mg/kg) on separate days in counterbalanced order, 30 minutes prior to a 60 minute test session.

Immunohistochemistry

To confirm viral injection location, mice were deeply anaesthetized using Beuthanasia (200 mg/kg, i.p.) and transcardially perfused with PBS followed by ice-cold 4% paraformaldehyde in PBS. Brains were fixed overnight in 4% paraformaldehyde in PBS then sliced at 40 µm thickness using a vibratome (Leica VT1000S). Free-floating coronal sections containing the NAc were incubated for 3hrs in blocking solution containing 0.2% Triton-X, 2% normal horse serum, and 0.05% Tween20. Sections were then incubated for 72 hrs with primary antibodies (mouse anti-mCherry 1:1000, Abcam; mouse anti-eYFP 1:1000, Abcam; rabbit anti-RFP 1:1000, Rockland), washed five times, and incubated overnight with secondary antibodies (donkey anti-rabbit Alexa Fluor 647 IgG 1:1000, Life Technologies; goat anti-mouse Alexa Fluor 488 or 647 IgG 1:1000, Abcam). Slides were washed and counter-stained for 20 minutes with 4',6-diamidino-2-phenylindole (DAPI) (1:50,000, Life Technologies), and mounted. Fluorescent images were acquired on a Keyence microscope using a 20x objective and viewed using ImageJ software.

Statistics

Analysis of variance (ANOVA) was conducted in IBM SPSS Statistics v24, using either one-way or factorial models as appropriate, and with repeated measures on within-subject factors. For main effects or interactions involving repeated measures, the Huynh-Feldt correction was applied to control for potential violations of the sphericity assumption. This correction reduces the degrees of freedom, resulting in non-integer

values. No significant main effects or interactions involving sex were observed, so data from male and female mice have been pooled for presentation. The Type I error rate was set to $\alpha = 0.05$ (two-tailed) for all comparisons. Effect sizes for significant results are expressed as partial eta-squared (η_p^2) values. All data are displayed as mean +/- SEM.

RESULTS

Behavioral Measures of Impulsivity and Attention in Mice

The 5-CSRT task requires mice to withhold a nose-poke response until it can be directed to one of five locations indicated by a brief visual cue (**Figure 1A**). Correct responses to the illuminated nose-poke aperture were rewarded with a food pellet, while all other trial outcomes were punished with a time-out period. These other outcomes included premature responses during the inter-trial interval (ITI) before cue presentation, incorrect responses to the wrong location, and omission trials in which the mouse fails to make a timely response. Training consisted of eight sequential stages of increasing ITI and decreasing cue durations (**Table 1**). To examine behavioral performance under varying degrees of task difficulty, we systematically varied the duration of either the visual cue (to test attention) or the ITI (to test impulsivity), as previously described (41). In a pilot study, we conducted these attention and impulsivity tests both early and late in training (**Figure 1B**). In the attention test, omission responses increased monotonically as the cue duration decreased ($F_{1.46,10.24} = 13.11$, $p = 0.002$, $\eta_p^2 = 0.65$), with little effect of training ($F_{1,7} < 1$; **Figure 1C**). In the impulsivity test, premature responses increased monotonically as the ITI grew longer ($F_{3,21} = 67.62$, $p < 0.001$, $\eta_p^2 = 0.91$), while the overall number of premature responses decreased with training ($F_{1,7} = 73.40$, $p < 0.001$, $\eta_p^2 = 0.91$;**Figure 1D**). We used this training protocol in subsequent experiments to investigate how FSIs in the NAc contribute to 5-CSRT task performance.

Characterization of FSIs in Mouse Nucleus Accumbens Core

To specifically target FSIs in the NAc core, we used a mouse line expressing Cre recombinase in a bicistronic fashion from the *Pvalb* locus (PV-2A-Cre). In this mouse line, Cre is active in cells with both high and low *Pvalb* expression (37), providing robust labeling of FSIs in both the dorsal striatum (32, 33) and NAc shell (22, 34). To characterize the properties of cells expressing Cre in the NAc core, we stereotaxically injected an

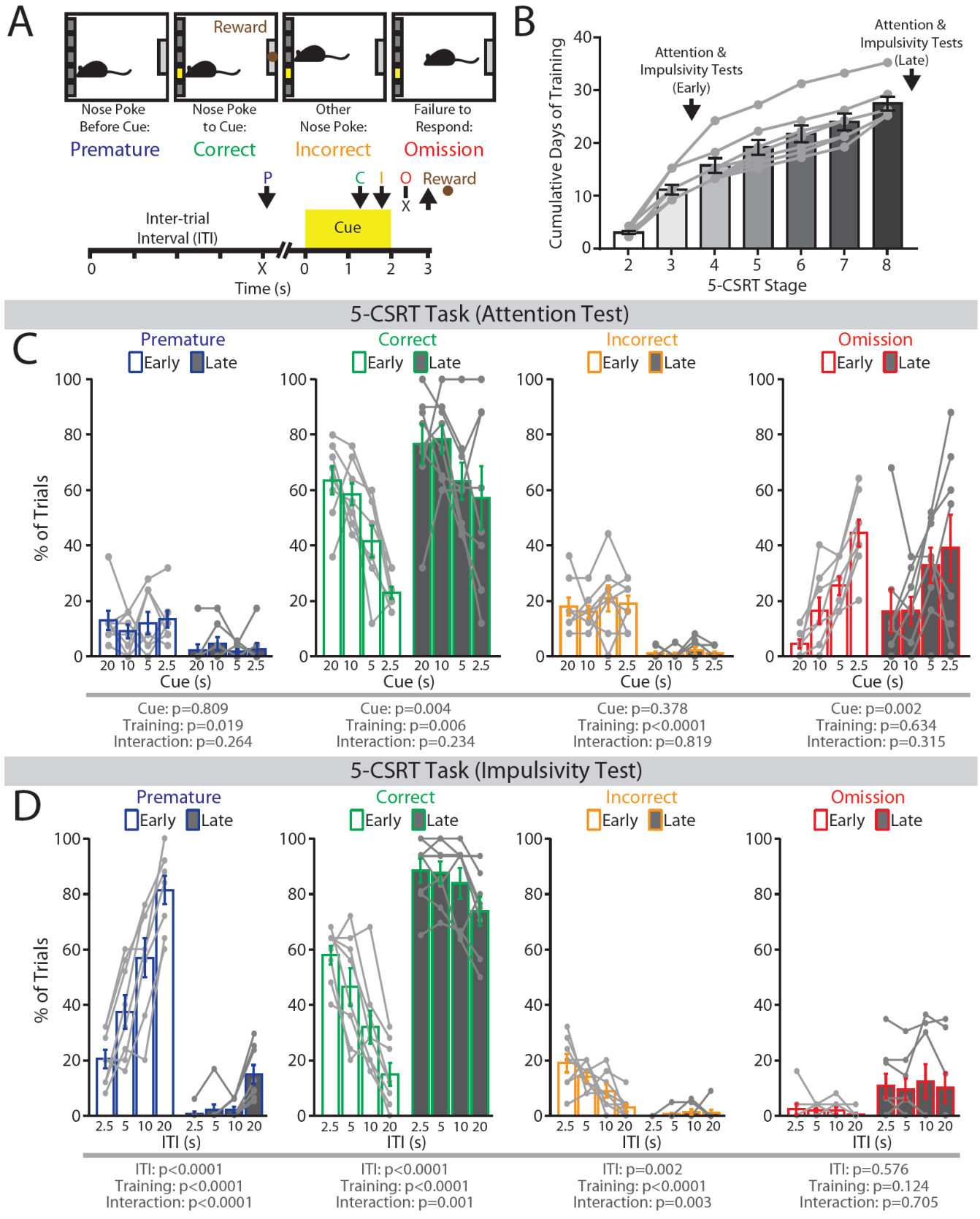

Figure 1. The 5-choice serial reaction time task in mice. (**A**) (**top**) *Trial outcomes in the 5-CSRT task. (**bottom**) Timeline of individual trials in the 5-CSRT task. Arrows indicate nose poke response. C, correct; I, incorrect; O, omission; P, premature. (**B**) Progression of mice in 5-CSRT task training. (**C**) In a test of attention at early and late training phases of the 5-CSRT task, percentage of premature, correct, incorrect, and omission trials varied by cue duration. (**D**) In a test of impulsivity at early and late training phases of the 5-CSRT task, the percentage of premature, correct, incorrect, and omission trials varied by ITI duration. n = 8 mice.*

adeno-associated virus (AAV) expressing red fluorescent protein in a Cre-dependent fashion (**Figure 2A**). We first carried out fluorescent *in situ* hybridization to co-label virally-expressed tdTomato with mRNA transcripts for parvalbumin (*Pvalb)* and parathyroid hormone like hormone (*Pthlh*), both of which are highly expressed in striatal FSIs (46, 47) (**Figure 2B**). The majority of virally-labelled (tdTomato+) cells expressed *Pvalb* and *Pthlh*, although the level of expression varied from cell to cell (**Figure 2C**). We occasionally observed virally-labelled (tdTomato+) cells with no detectable *Pvalb* or *Pthlh* expression, as previously reported in this mouse line (34, 48). To confirm that these cells were indeed FSIs, we performed whole-cell patch-clamp recordings from virally-labelled cells in acute NAc brain slices. In current-clamp recordings, these cells showed characteristic properties of FSIs (**Figure**

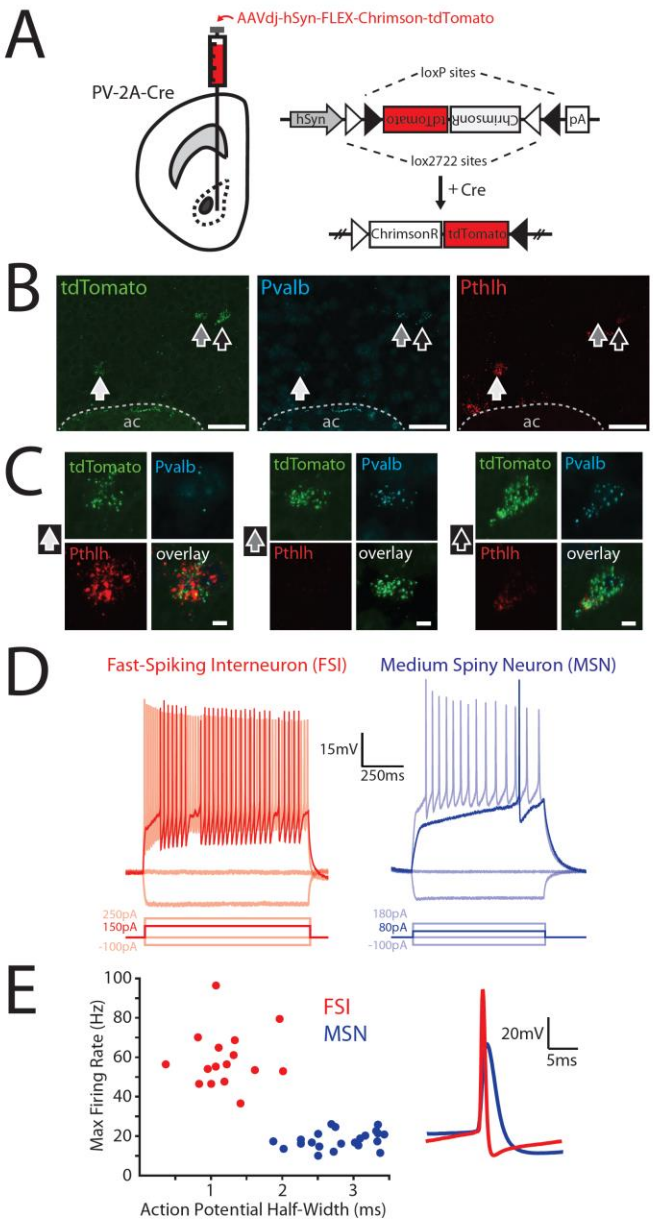

Figure 2. Electrophysiological and transcriptional characterization of FSIs in the NAc core*. (**A**) Viral strategy for labeling FSIs in PV-2A-Cre mice: flip-excision (FLEX) constructs are inverted and expressed by cells containing Cre recombinase. Note that bicistronic expression of ChrimsonR is not relevant for this experiment, but is useful for subsequent experiments (see Figure 3). (**B**) In situ hybridization of gene transcripts indicating co-expression of virally-expressed TdTomato (green) with Pvalb (cyan) and Pthlth (red) (scale bar, 50 µm; ac, anterior commissure). Arrows indicate cells in (D). (**C**) High magnification images highlighting variability in Pvalb and Pthlh expression (scale bar, 5 µm). (**D**) Current-clamp recordings from (**left**) FSIs (red) and (**right**) medium spiny neurons (MSNs; blue) at regular current steps. Bolded step indicates lowest input current needed to elicit spiking (rheobase). (**E**) (**left**) Scatterplot of spike width at half amplitude (x) and maximum firing rate (y) for FSIs (red, n = 16) and MSNs (blue, n = 23). (**right**) Action potential waveforms of a representative FSI and MSN.*

2D), including a high maximum firing rate, narrow action potential half-width, and short-duration afterhyperpolarization (49). These electrophysiological properties could be easily distinguished from those of medium spiny projection neurons (MSNs), the most abundant type of neuron in the NAc (**Figure 2E**). These data confirm that our viral targeting approach specifically labels FSIs in the NAc core.

Optogenetically-Evoked Calcium Signal in FSIs and MSNs

Our next objective was to characterize endogenous patterns of FSI activity in the NAc of freely behaving mice. Due to the limited number and sparse distribution of FSIs in the NAc, we used fiber photometry to collect bulk calcium signal from FSI ensembles within a large tissue volume (50, 51). PV-2A-Cre mice were stereotaxically co-injected with two AAVs expressing Cre-dependent constructs: the genetically-encoded calcium indicator jGCaMP7s (52), and the red-shifted excitatory opsin ChrimsonR (53). A chronic fiber-optic implant was placed in the NAc just above the site of virus injection, and was used to both deliver excitation light and collect emitted fluorescence (**Figure 3A**). Immunohistochemical examination of infected brain slices revealed sparse and overlapping viral co-expression, as well as proximal placement of fiber optic implant (**Figure 3B**).

To confirm that reliable fiber photometry signals could be recorded from sparsely distributed FSIs in the NAc, we tethered freely moving mice to the fiber photometry system and delivered amber light (594 nm) through the fiber-optic implant to activate ChrimsonR (**Figure 3C**). We detected robust jGCaMP7s signals that varied in a dose-dependent fashion with stimulation frequency ($F_{1.61,9.64} = 8.13$, $p = 0.011$, $\eta_p^2 = 0.58$; **Figure 3D**), pulse number ($F_{2.72,16.35} = 5.72$, $p = 0.008$, $\eta_p^2 = 0.49$; **Figure 3E**), and light power ($F_{1.82,10.89} = 12.84$, $p = 0.002$; $\eta_p^2 = 0.68$; **Figure 3F**). In a separate group of mice, we also used fiber photometry to evaluate the effect of FSI activation on neighboring MSNs. PV-2A-Cre mice were co-injected with AAVs encoding Cre-dependent ChrimsonR (expressed in FSIs), as well as Cre-*inactivated* jGCaMP7s with a CaMKII promoter to drive expression in MSNs (46) (**Figure 3G,H**). This strategy allowed for red-shifted optogenetic excitation of FSIs with concurrent fiber photometry monitoring of MSN responses. In mice receiving amber light stimulation at 20 Hz, we observed a significant reduction in calcium signal ($F_{1,3} = 15.00$, $p = 0.030$, $\eta_p^2 = 0.83$; **Figure 3I**), suggesting an inhibitory action of FSIs onto neighboring MSNs within the NAc core.

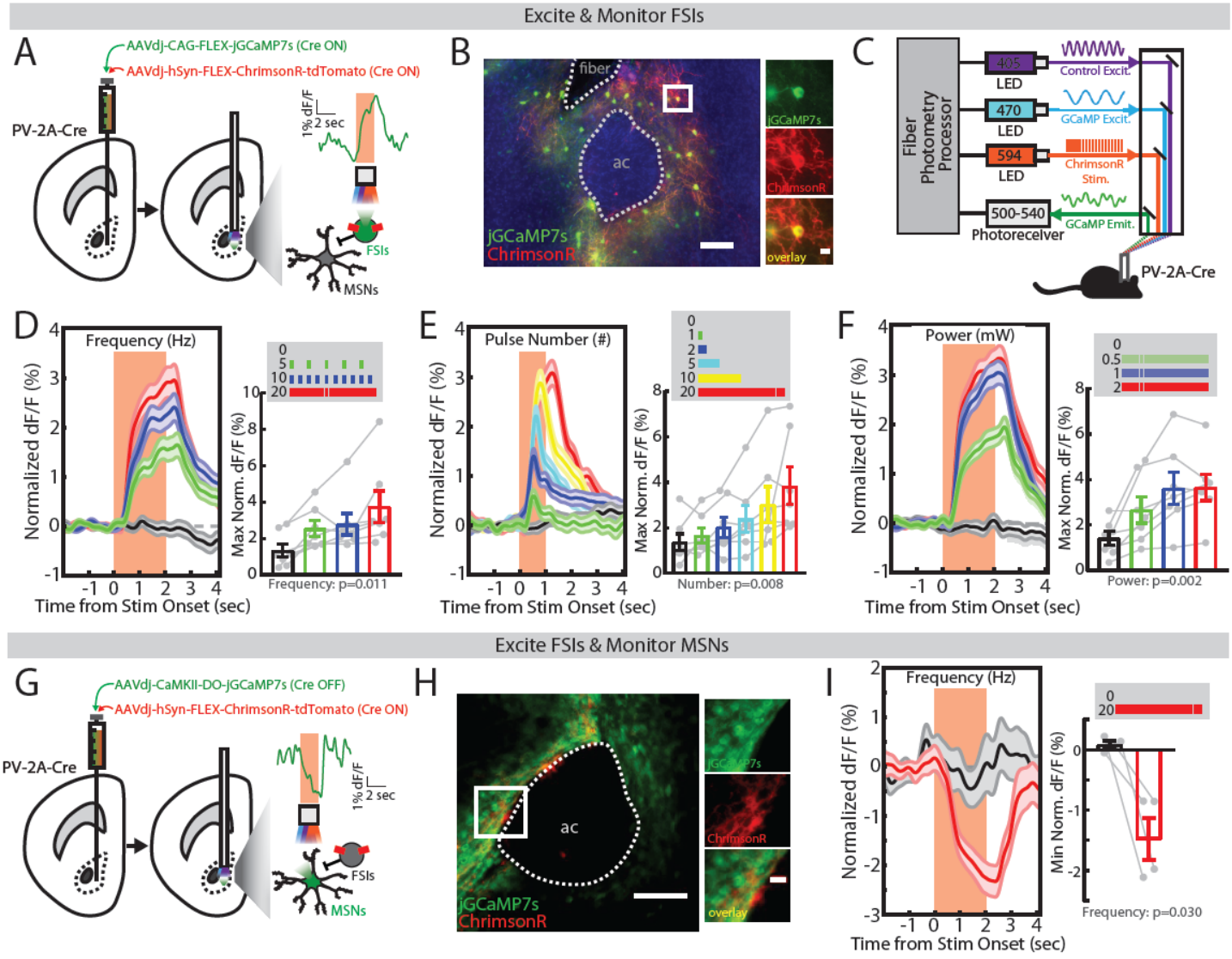

Figure 3. Optogenetically-evoked calcium signals from FSIs and MSNs in the NAc core. *(**A**) Viral injection of Cre-dependent ChrimsonR and jGCaMP7s into the NAc core of PV-2A-Cre mice (n = 7). Inset shows photometry signal on a single representative trial. (**B**) (**left**) Visualization of fiber photometry implant placed above FSIs co-expressing ChrimsonR (red) and jGCaMP7s (green) (ac, anterior commissure; scale bar, 100 µm). (**right**) Magnified image of a single FSI (scale bar, 10 µm). (**C**) Setup for simultaneous in vivo optogenetic excitation and fiber photometry monitoring. In vivo optogenetically-evoked jGCaMP7s signal measured by varying (**D**) stimulation frequency (0, 5, 10, 20 Hz; n = 20 trials each), (**E**) pulse number (0, 1, 2, 5, 10, 20; n = 20 trials each), or (**F**) light power (0, 0.5, 1, 2 mW; n = 20 trials each). (**G**) Viral injection of Cre-dependent ChrimsonR and Cre-inactivated jGCaMP7s into the NAc core of PV-2A-Cre mice (n = 4). Inset shows photometry signal on a single representative trial. (**H**) (**left**) Visualization of non-overlapping expression of ChrimsonR (red) and jGCaMP7s (green) in FSIs and putative MSNs, respectively (ac, anterior commissure; scale bar, 100 µm). (**right**) Magnified image illustrating non-overlapping expression (scale bar, 10 µm). (**I**) Optogenetic excitation of FSIs significantly reduces jGCaMP7s signal from putative MSNs.*

Fiber Photometry Monitoring of FSIs during the 5-CSRT Task

Having validated the specificity and reliability of the fiber photometry signal from FSIs in the NAc, we proceeded to record this signal while mice performed the 5-CSRT task. Experimental mice included those with validated jGCaMP7s expression from the preceding optogenetic experiments (see Figure 3), as well as a control

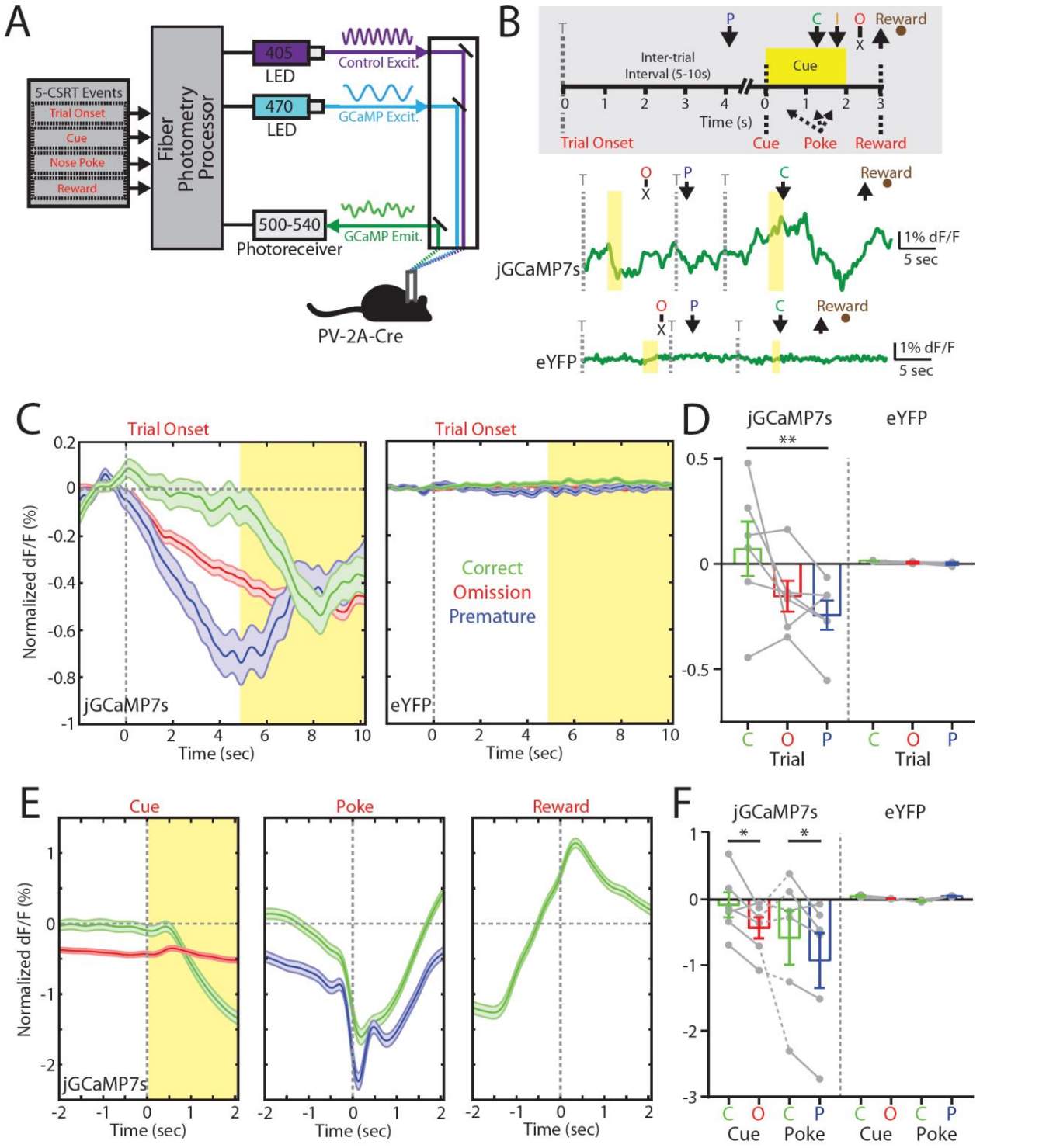

Figure 4. FSI activity within the NAc core predicts trial outcome in the 5-CSRT task. (***A***) *Fiber photometry setup for in vivo monitoring of jGCaMP7s expressed by FSIs during the 5-CSRT task. (**B**) (**top**) Timeline of the 5-CSRT task, including events for fiber photometry analysis. Arrows indicate nose poke response. C, correct; I, incorrect; O, omission; P, premature; T, trial onset. (**bottom**) Example fiber photometry signal across various trial types in PV-2A-Cre mice expressing jGCaMP7s or eYFP. (**C**) Combined fiber photometry data normalized to trial onset for mice expressing (**left**) jGCaMP7s (trials: correct, 919; premature, 425; omission, 4871) and (**right**) eYFP (trials: correct, 678; premature, 177; omission, 1789). Yellow boxes indicate possible cue period. (**D**) Fiber photometry data averaged within animal. (**E**) Combined fiber photometry data for mice expressing jGCaMP7s normalized to trial onset and aligned to (**left**) cue, (**middle**) nose poke response, and (**right**) magazine entry for food reward. (**F**) Fiber photometry data averaged within animal. Bar graphs represent normalized dF/F values averaged over two seconds prior to (cue, poke) or following (trial) each aligned event. * p < 0.05; ** p < 0.01.*

cohort of PV-2A-Cre mice infected with a Cre-dependent eYFP fluorophore. Upon reaching the final stage of testing, we collected fiber photometry data across five consecutive sessions, with simultaneous excitation of jGCaMP7s at a calcium-dependent wavelength (470 nm), as well as an isosbestic wavelength (405 nm) used to correct for bleaching and movement artifact (**Figure 4A**). Behavioral responses in the 5-CSRT task were time-locked to the fiber photometry signal using TTL outputs from the operant chamber control software (**Figure 4B**).

We first examined fiber photometry signals aligned to trial onset, which coincided with the beginning of the ITI period (**Figure 4C, left**). FSI activity was sustained throughout the ITI on correct trials, whereas it declined throughout the ITI on both omission and premature trials. These response profiles were absent in control mice expressing the eYFP fluorophore (**Figure 4C, right**), indicating that motion or other artifacts did not contribute to jGCaMP7s signal. Calcium signal averaged within experimental animal indicated a significant difference in FSI activity following the onset of correct versus premature trials in jGCaMP7s-expressing mice ($F_{1,5} = 16.18$, $p = 0.010$, $\eta_p^2 = 0.76$), but the difference between correct and omission trials was not statistically significant ($F_{1,5} = 2.84$, $p = 0.15$, $\eta_p^2 = 0.36$; **Figure 4D**). In mice expressing jGCaMP7s, elevated FSI activity on correct trials was sustained until cue presentation (**Figure 4E, left**). Signal alignment to nose poke response showed elevated FSI activity before correct versus premature responses (**Figure 4E, middle**). There was no evidence that this signal varied as a function of spatial location relative to implanted hemisphere (**Supplementary Figure S1**). Lastly, signal alignment to magazine entry after correct responses revealed an increase in FSI activity associated with food pellet retrieval (**Figure 4E, right**). After averaging calcium signals within animal, we observed significant increases in FSI activity before cue presentation on correct versus omission trials ($F_{1,5} = 7.46$, $p = 0.041$, $\eta_p^2 = 0.60$), as well as before the nose poke response on correct versus premature trials ($F_{1,5} = 7.68$, $p = 0.039$, $\eta_p^2 = 0.61$; **Figure 4F**). Incorrect responses were not analyzed, as they represented a negligible proportion of all trials (1.6 and 1.8% from jGCaMP7s and eYFP mice, respectively). Altogether, these data suggest that FSI activity shapes the selection and timing of behavioral responses in the 5-CSRT task, and reductions of FSI activity predict poor behavioral performance in the form of omissions or premature responses.

Chemogenetic Inhibition of FSIs Increases Impulsivity

Given the relationship between FSI activity and behavioral performance in the 5-CSRT task, we sought to directly manipulate FSI activity levels *in vivo* using a chemogenetic strategy, and determine the behavioral

consequences. Prior to the start of 5-CSRT task training, PV-2A-Cre mice and wild-type littermates received bilateral injections of an AAV expressing Cre-dependent hM4Di in the NAc core (**Figure 5A**). This Gi-DREADD (Designer Receptor Exclusively Activated by Designer Drugs) can be activated by clozapine-N-oxide (CNO), initiating intracellular signaling cascades that reduce neuronal excitability (54). To validate the effect of this manipulation on FSIs in the NAc core, we performed current-clamp recordings from virally-labeled FSIs in acute brain slices, and measured electrophysiological properties before and after bath application of CNO (3 μM; **Figure 5B**). CNO caused a significant reduction in maximum firing rate ($F_{1,14}$ = 5.73, p = 0.031, η_p^2 = 0.29), as

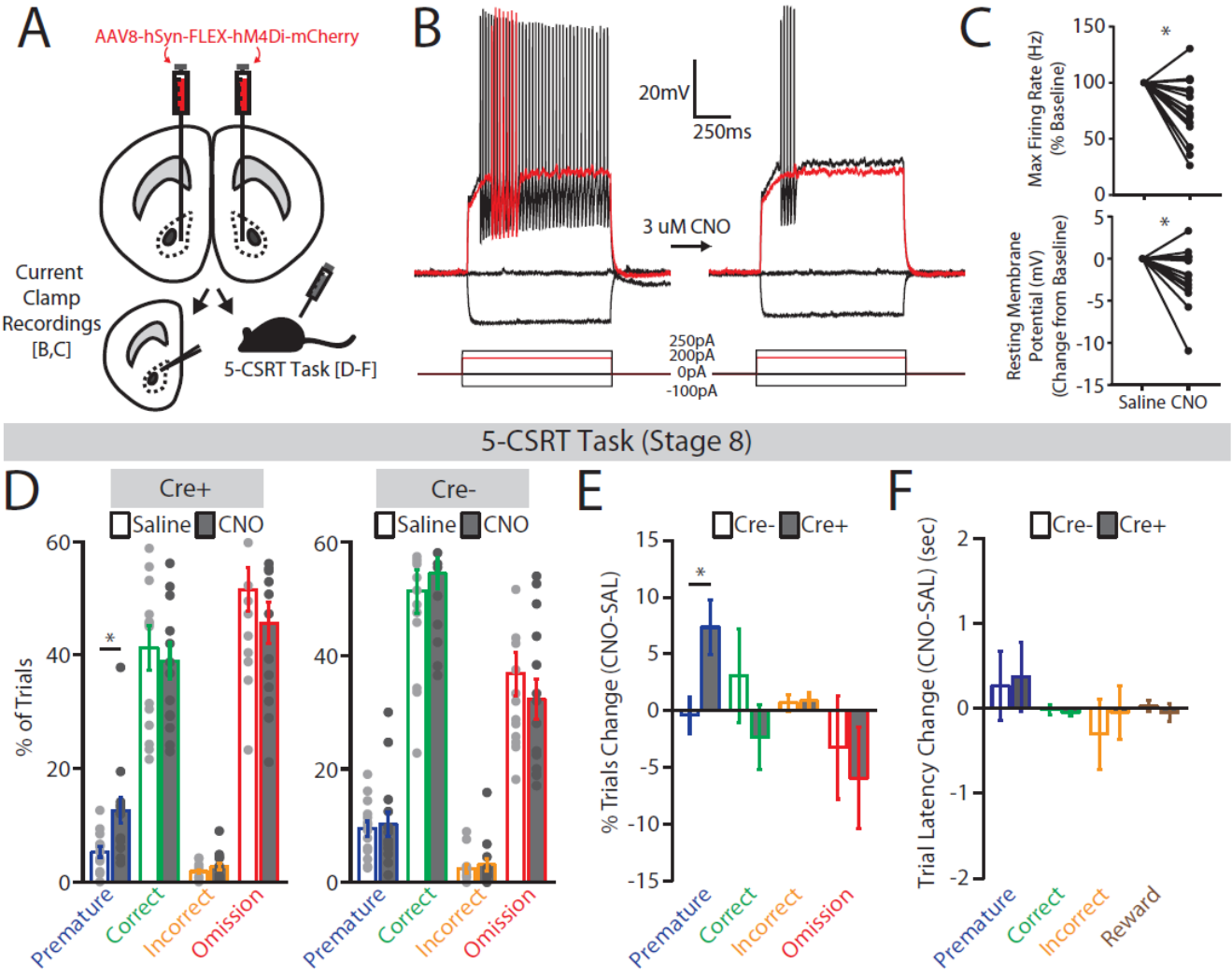

Figure 5. Inactivation of FSIs increases impulsive behavior in the terminal stage of the 5-CSRT task*. (**A**) Bilateral viral injection of Cre-dependent hM4Di into the NAc core of PV-2A-Cre or wild-type mice for electrophysiological validation or 5-CSRT task behavior. (**B**) Whole-cell current-clamp recording of a representative FSI before and after bath application of CNO (3 μM). Red trace indicates lowest input current needed to elicit spiking (rheobase) before CNO application. (**C**) (**top**) Chemogenetic inhibition reduces maximum spiking rate of FSIs and (**bottom**) overall resting membrane potential (n = 15 cells). (**D**) Raw trial outcomes for the final stage of the 5-CSRT task in (**left**) PV-2A-Cre (n = 14) and (**right**) wild-type (n = 14) mice following injection of saline or CNO (2 mg/kg). (**E**) Systemic administration of CNO (2 mg/kg) selectively increased the percentage of premature trials in PV-2A-Cre mice expressing hM4Di, but (**F**) did not influence response or reward retrieval latencies. * p < 0.05.*

well as hyperpolarization of the resting membrane potential ($F_{1,14}$ = 5.09, p = 0.041, η_p^2 = 0.27; **Figure 5C, Supplementary Figure S2**). These effects in acute brain slices were further corroborated using fiber photometry to verify chemogenetic inhibition of FSIs *in vivo* (**Supplementary Figure S3**).

After bilateral injection of AAV-FLEX-hM4Di virus into the NAc core, PV-2A-Cre mice and wild-type littermates were trained on the 5-CSRT task. Upon reaching the last stage of training, we injected either saline or CNO (2 mg/kg) thirty minutes before testing on separate days. In PV-2A-Cre mice, injection of CNO caused a significant increase in the percentage of premature trials, relative to saline ($F_{1,13}$ = 9.15, p = 0.010, η_p^2 = 0.41; **Figure 5D, left**). This effect was not observed in wild-type littermates ($F_{1,13}$ < 1; **Figure 5D, right**), confirming that the effects of CNO were only observed following viral expression of hM4Di in FSIs. This elevation of premature responding was also robust when comparing difference scores (CNO-saline) between genotypes ($F_{1,26}$ = 7.08, p = 0.013, η_p^2 = 0.21; **Figure 5E**), but there were no significant changes in the percentage of other trials types. There was also no change in the number of perseverative responses following injection of CNO versus saline in either genotype (PV-2A-Cre: 1.71±1.76; wild-type: 2.86±1.13; $F_{1,26}$ < 1). Importantly, chemogenetic modulation of FSIs did not affect latencies to respond or retrieve reward ($F_{1,26}$ < 1; **Figure 5F**), nor did it alter locomotor activity in an open field (**Supplementary Figure S4**).

After determining the effect of chemogenetic FSI inhibition in the final training stage, this same cohort of mice was run through the attention and impulsivity tests described in **Figure 1**, with injection of saline or CNO (2 mg/kg) thirty minutes before each test session. In the attention test, there was an increase in correct trials following CNO injection in PV-2A-Cre mice ($F_{1,13}$ = 5.68, p = 0.033, η_p^2 = 0.30; **Figure 6A**). Although there was a numerical trend for these mice to have fewer omissions after CNO ($F_{1,13}$ = 4.04, p = 0.066), this was not significantly different from wild-type mice (genotype: $F_{1,13}$ = 2.71, p = 0.11; **Figure 6B; Supplementary Figure S5**). Strikingly, in the impulsivity test, administration of CNO increased the percentage of premature trials in PV-2A-Cre mice when the ITI was long (Treatment x ITI interaction: $F_{2.16,28.10}$ = 9.76, p < 0.001, η_p^2 = 0.43; **Figure 6C**). These effects of CNO were dependent on hM4Di expression in NAc FSIs (Genotype x ITI interaction: $F_{2.34,60.89}$ = 3.58, p = 0.028, η_p^2 = 0.12; **Figure 6D**), as there were no behavioral differences between CNO and saline injection in the wild-type littermate control group (**Supplementary Figure S6)**. Collectively, these data suggest FSIs in the NAc core normally constrain premature responses in the 5-CSRT task, and that disruption of FSI function can lead to impulsive behavior.

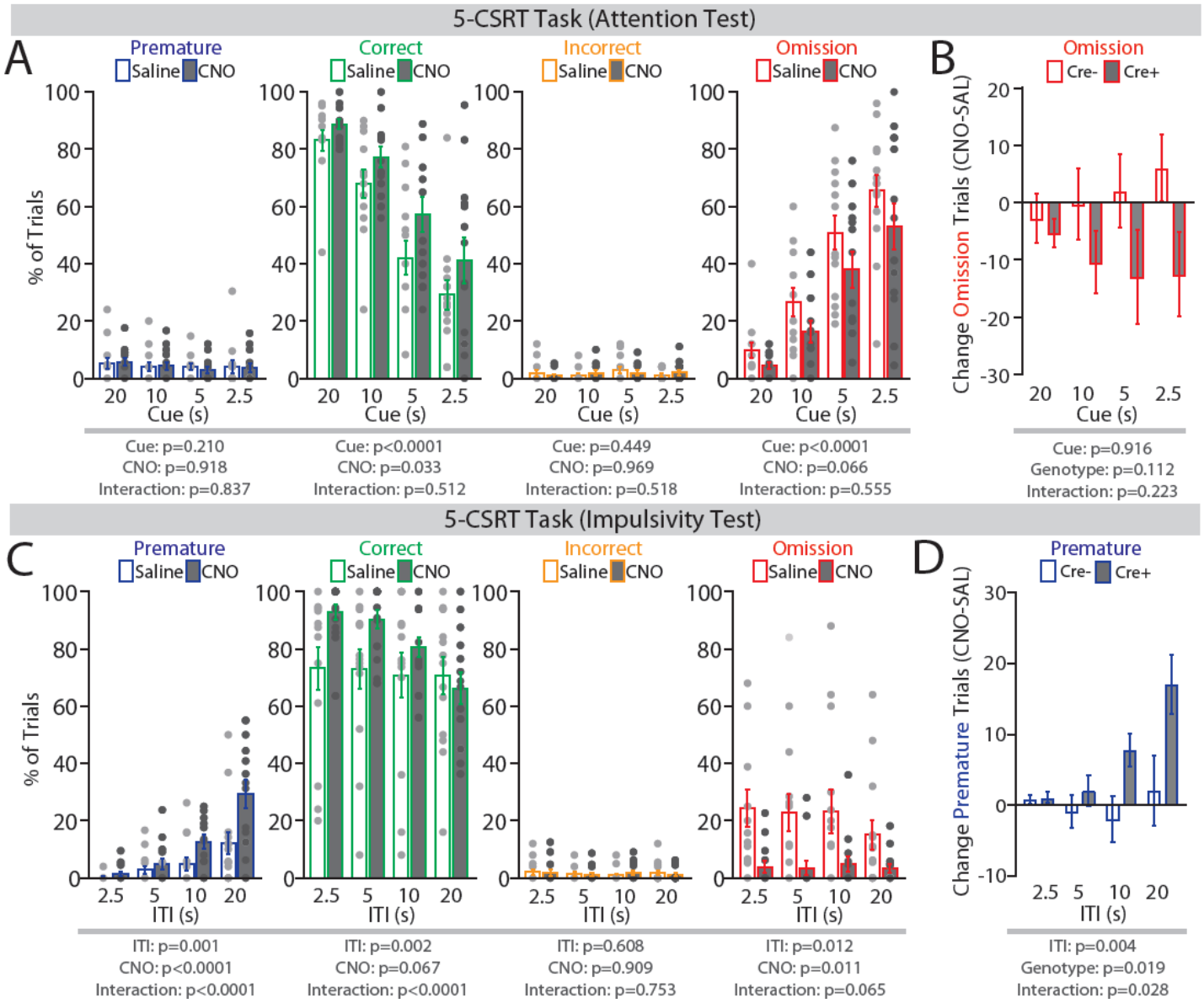

Figure 6. Inactivation of FSIs selectively promotes impulsive action in the 5-CSRT task (impulsivity and attention tests). *(**A**) In PV-2A-Cre mice performing a test of attention, systemic administration of CNO (2 mg/kg.) increased the percentage of correct trials but did not significantly affect the percentage of premature, incorrect, or omission trials. (**B**) There was no difference in percentage of omission trials between PV-2A-Cre and wild-type mice following CNO administration. (**C**) In PV-2A-Cre mice performing a test of impulsivity, systemic administration of CNO (2mg/kg) significantly increased the percentage of premature and correct trials, but did not influence incorrect trials, and decreased omission trials. (**D**) The increased percentage of premature trials following CNO administration in PV-2A-Cre was significantly different from wild-type littermates. n = 14 mice per genotype.*

DISCUSSION

Decades of research clearly implicate the NAc in controlling multiple facets of impulsivity, but the contribution of specific cell types within this heterogeneous brain region has remained unclear. In this study, we focused on the contribution of FSIs, which are few in number but exert powerful inhibitory control over MSN output from the NAc (22–24). We used PV-2A-Cre transgenic mice to monitor and manipulate the activity of FSIs

in the NAc core. Our data suggest the sustained activity of these cells positively correlates with successful control of impulsive behavior in the 5-CSRT task. Furthermore, using chemogenetic methods to directly inhibit FSIs in the NAc core, we observed enhanced impulsivity across a range of task conditions. These findings indicate FSIs in the NAc core play a key role in impulse control.

The sparse distribution of FSIs in the NAc has historically made these cells difficult to study. FSIs represent fewer than 1% of all neurons in the dorsal striatum of rodents (55), with immunohistochemical and electrophysiological evidence suggesting FSIs are even less abundant in the NAc (56, 57). Several aspects of our experimental design facilitated analysis of these scarce interneurons, including bulk calcium imaging of NAc tissue with fiber photometry. We sought to maximize the fluorescent signal from FSIs by virally expressing jGCaMP7s, a recently developed and highly sensitive genetically encoded calcium indicator (52). Using red-shifted optogenetic excitation with ChrimsonR, we confirmed the sensitivity of this method for measuring FSI activation in the NAc core. It should be noted that the kinetics of jGCaMP7s activation and bulk nature of fiber photometry cannot resolve specific spiking patterns of individual FSIs, but instead provide an aggregate view of FSI activation.

This fiber photometry approach enabled real-time monitoring of FSI activity in the NAc core as mice performed the 5-CSRT task. On correct trials, FSI activity was sustained during the ITI, then declined after cue presentation and nose poke in the appropriate location. In contrast, FSI activity declined during the ITI on omission and premature trials, and remained low at the time of premature response (premature trials) or cue presentation (omission trials). This finding raised two possibilities: FSI activity prevents premature responses and/or sustains attention prior to cue presentation. To differentiate these possibilities and move beyond correlations between FSI activity and behavior, we used a chemogenetic approach to directly and specifically inhibit the activity of FSIs in the NAc core. This manipulation increased the frequency of premature responses, especially with long ITI periods, strongly linking FSI activity with successful impulse control. Importantly, CNO injection had no effect in wild-type control animals, demonstrating the behavioral effects of this designer drug depended on hM4Di DREADD expression in NAc FSIs.

Compared to effects on impulsivity, chemogenetic inhibition of FSIs in the NAc had no significant effects on omission responses late in training or in the attention test. However, this manipulation improved performance in the impulsivity test when the ITI was short, due to a significant *decrease* in omissions. This contrasts with the

behavioral function of FSIs in the prefrontal cortex, which are also active during the ITI and appear to sustain attention in the 5-CSRT task (31). It is thus striking that the same cell type in different brain regions has seemingly distinct behavioral functions, especially given that connections between the prefrontal cortex and NAc are involved in 5-CSRT task performance (13). This surprising result makes sense if FSIs in the prefrontal cortex inhibit the activity of pyramidal cells that project to the NAc, thereby reducing excitatory drive to FSIs (58–60). The control of attention by FSIs in the prefrontal cortex (31) may also involve regulation of pyramidal cells that project to other brain regions, such as the dorsomedial striatum (61) or the claustrum (62).

Our ability to monitor and manipulate FSIs in the NAc core was facilitated by use of the PV-2A-Cre mouse line, which labels cells with both high and low expression of Pvalb (37). The high penetrance of Cre expression in this mouse line appears to be critical for labeling the majority of FSIs in the NAc (22) and dorsal striatum (32). To confirm this high penetrance did not reduce the specificity of Cre expression in FSIs, we performed electrophysiological characterization of virally-infected cells in acute brain slices. All of the cells we recorded exhibited characteristic properties of FSIs, consistent with another recent study in the NAc (22). However, *in situ* hybridization revealed variable expression of *Pvalb* transcript, including a small number of cells that lacked detectable *Pvalb* expression. Similar findings with this mouse line have previously been reported in both NAc (34) and hippocampus (48), but electrophysiological data nevertheless suggests these cells are FSIs. The level of *Pvalb* expression in these cells may be below the threshold of detection with *in situ* hybridization, while still providing a small amount of Cre expression necessary to activate Cre-dependent viral constructs. FSIs with little *Pvalb* may be more readily labelled by other markers, such as *Pthlh* (47) or cannabinoid receptor type 1 (63).

FSIs form strong inhibitory synaptic connections onto MSNs in the NAc (22, 24, 63). Using fiber photometry, we found that optogenetic stimulation of FSIs in the NAc core decreased the calcium signal detected from surrounding MSNs, consistent with a net inhibitory influence of NAc FSIs on MSN activity *in vivo*. The increased impulsivity observed after chemogenetic FSI inhibition is thus likely to involve disinhibition of NAc output from MSNs. We speculate that the amount of GABA released by FSIs onto MSNs may be a key factor controlling impulsivity, since highly impulsive rats have decreased NAc GABA levels (19), but no change in NAc GABA receptor binding (64). Highly impulsive rats also have lower expression of glutamate decarboxylase in the NAc core (18), and this key GABA synthetic enzyme is encoded by two genes (*Gad1* and *Gad2*) expressed at

high levels by striatal FSIs (46). Reduced GABA synthesis by FSIs may thus contribute to increased impulsivity observed after local knockdown of glutamate decarboxylase expression in the NAc core (18).

The synaptic and molecular mechanisms by which NAc FSIs regulate impulsivity will be an important topic for future research, since FSI dysfunction is linked to numerous neuropsychiatric disorders (65, 66). Tourette's syndrome, a disorder associated with loss of motoric inhibitory control, presents with loss of striatal FSIs (67). Experimental disruption of FSIs in the dorsal striatum can also produce abnormal behaviors in animal models, including stereotypies and dyskinesias (68–71). In the NAc, FSI manipulation alter behavioral responses to addictive drugs (34, 35). Thus, the present findings have broad implications for understanding addiction (8, 72) and other neuropsychiatric disorders (2, 11) epitomized by deficits in impulse control and associated dysfunction of limbic neurocircuitry.

ACKNOWLEDGEMENTS

Research reported in this publication was supported by the University of Minnesota's MnDRIVE (Minnesota's Discovery, Research and Innovation Economy) initiative (to MTP and PER), as well as grants from the National Institutes of Health (F32MH118794 to MTP and R00DA037279 to PER) and the Whitehall Foundation, a NARSAD Young Investigator Grant from the Brain & Behavior Research Foundation, and an MQ Fellows Award (all to PER). Some of the viral vectors used in this study were generated by the University of Minnesota Viral Vector and Cloning Core, as well as the Stanford University Gene Virus and Vector Core. We thank Justin Lines for fiber photometry analysis troubleshooting, Eshaan Iyer for early piloting of the 5-CSRT task, Sowmya Narayan and Sumyuktha Vijay for assistance with behavioral experiments, David Leipold for maintenance of mouse colonies, and Carlee Toddes and Dieter Brandner for helpful discussion of the manuscript.

DISCLOSURES

The authors declare no competing financial interests.

REFERENCES

1. Dalley JW, Everitt BJ, Robbins TW (2011): Impulsivity, compulsivity, and top-down cognitive control. *Neuron*. 69: 680–694.
2. Dalley JW, Robbins TW (2017): Fractionating impulsivity: Neuropsychiatric implications. *Nat Rev Neurosci*. 18: 158–171.
3. Verdejo-García A, Lawrence AJ, Clark L (2008): Impulsivity as a vulnerability marker for substance-use disorders: Review of findings from high-risk research, problem gamblers and genetic association studies. *Neurosci Biobehav Rev*. 32: 777–810.
4. Winstanley CA, Eagle DM, Robbins TW (2006): Behavioral models of impulsivity in relation to ADHD: Translation between clinical and preclinical studies. *Clin Psychol Rev*. 26: 379–395.
5. Chamberlain SR, Robbins TW, Winder-Rhodes S, Mller U, Sahakian BJ, Blackwell AD, Barnett JH (2011): Translational approaches to frontostriatal dysfunction in attention-deficit/hyperactivity disorder using a computerized neuropsychological battery. *Biol Psychiatry*. 69: 1192–1203.
6. Javdani S, Sadeh N, Verona E (2011): Suicidality as a function of impulsivity, callous-unemotional traits, and depressive symptoms in youth. *J Abnorm Psychol*. 120: 400–413.
7. Basar K, Sesia T, Groenewegen H, Steinbusch HWM, Visser-Vandewalle V, Temel Y (2010): Nucleus accumbens and impulsivity. *Prog Neurobiol*. 92: 533–557.
8. Morris LS, Kundu P, Baek K, Irvine MA, Mechelmans DJ, Wood J, *et al.* (2016): Jumping the gun: Mapping neural correlates of waiting impulsivity and relevance across alcohol misuse. *Biol Psychiatry*. 79: 499–507.
9. Kable JW, Glimcher PW (2007): The neural correlates of subjective value during intertemporal choice. *Nat Neurosci*. 10: 1625–1633.
10. McClure SM (2004): Separate neural systems value immediate and delayed monetary rewards. *Science (80-)*. 306: 503–508.
11. Carmona S, Proal E, Hoekzema EA, Gispert JD, Picado M, Moreno I, *et al.* (2009): Ventro-striatal reductions underpin symptoms of hyperactivity and impulsivity in attention-deficit/hyperactivity disorder. *Biol Psychiatry*. 66: 972–977.
12. Cardinal RN, Pennicott DR, Lakmali C, Robbins TW, Everitt BJ (2001): Impulsive choice induced in rats by lesions of the nucleus accumbens core. *Science (80-)*. 292: 2499–2501.
13. Christakou A (2004): Prefrontal cortical-ventral striatal interactions involved in affective modulation of attentional performance: implications for corticostriatal circuit function. *J Neurosci*. 24: 773–780.
14. Pothuizen HHJ, Jongen-Rêlo AL, Feldon J, Yee BK (2005): Double dissociation of the effects of selective nucleus accumbens core and shell lesions on impulsive-choice behaviour and salience learning in rats. *Eur J Neurosci*. 22: 2605–2616.
15. Murphy ER, Robinson ESJ, Theobald DEH, Dalley JW, Robbins TW (2008): Contrasting effects of selective lesions of nucleus accumbens core or shell on inhibitory control and amphetamine-induced impulsive behaviour. *Eur J Neurosci*. 28: 353–363.
16. Koskinen T, Sirviö J (2001): Studies on the involvement of the dopaminergic system in the 5-HT2agonist (DOI)-induced premature responding in a five-choice serial reaction time task. *Brain Res Bull*. 54: 65–75.
17. Pezze MA, Dalley JW, Robbins TW (2007): Differential roles of dopamine D1 and D2 receptors in the nucleus accumbens in attentional performance on the five-choice serial reaction time task. *Neuropsychopharmacology*. 32: 273–283.
18. Caprioli D, Sawiak SJ, Merlo E, Theobald DEH, Spoelder M, Jupp B, *et al.* (2014): Gamma aminobutyric acidergic and neuronal structural markers in the nucleus accumbens core underlie trait-like impulsive behavior. *Biol Psychiatry*. 75: 115–123.
19. Sawiak SJ, Jupp B, Taylor T, Caprioli D, Carpenter TA, Dalley JW (2016): In vivo γ-aminobutyric acid measurement in rats with spectral editing at 4.7T. *J Magn Reson Imaging*. 43: 1308–1312.
20. Hayes DJ, Jupp B, Sawiak SJ, Merlo E, Caprioli D, Dalley JW (2014): Brain γ-aminobutyric acid: A neglected role in impulsivity. *Eur J Neurosci*. 39: 1921–1932.
21. Hu H, Gan J, Jonas P (2014): Fast-spiking, parvalbumin+ GABAergic interneurons: From cellular design to microcircuit function. *Science (80-)*. 345. doi: 10.1126/science.1255263.
22. Scudder SL, Baimel C, Macdonald EE, Carter AG (2018): Hippocampal-evoked feed-forward inhibition in the nucleus accumbens. *J Neurosci*. 38: 1971–18.
23. Wright WJ, Schlüter OM, Dong Y (2017): A feedforward inhibitory circuit mediated by CB1-expressing fast-spiking interneurons in the nucleus accumbens. *Neuropsychopharmacology*. 42: 1146–1156.

24. Taverna S, Canciani B, Pennartz CMA (2007): Membrane properties and synaptic connectivity of fast-spiking interneurons in rat ventral striatum. *Brain Res*. 1152: 49–56.
25. Koós T, Tepper JM (1999): Inhibitory control of neostriatal projection neurons by GABAergic interneurons. *Nat Neurosci*. 2: 467–472.
26. Straub C, Saulnier JL, Bègue A, Feng DD, Huang KW, Sabatini BL (2016): Principles of synaptic organization of GABAergic interneurons in the striatum. *Neuron*. 92: 84–92.
27. Gittis AH, Nelson AB, Thwin MT, Palop JJ, Kreitzer AC (2010): Distinct roles of GABAergic interneurons in the regulation of striatal output pathways. *J Neurosci*. 30: 2223–34.
28. Cardin JA, Carlén M, Meletis K, Knoblich U, Zhang F, Deisseroth K, *et al.* (2009): Driving fast-spiking cells induces gamma rhythm and controls sensory responses. *Nature*. 459: 663–667.
29. Royer S, Zemelman B V., Losonczy A, Kim J, Chance F, Magee JC, Buzsáki G (2012): Control of timing, rate and bursts of hippocampal place cells by dendritic and somatic inhibition. *Nat Neurosci*. 15: 769–775.
30. Sohal VS, Zhang F, Yizhar O, Deisseroth K (2009): Parvalbumin neurons and gamma rhythms enhance cortical circuit performance. *Nature*. 459: 698–702.
31. Kim H, Ährlund-Richter S, Wang X, Deisseroth K, Carlén M (2016): Prefrontal parvalbumin neurons in control of attention. *Cell*. 164: 208–218.
32. Owen SF, Berke JD, Kreitzer AC (2018): Fast-spiking interneurons supply feedforward control of bursting, calcium, and plasticity for efficient learning. *Cell*. 172: 683–695.e15.
33. O'Hare JK, Li H, Kim N, Gaidis E, Ade K, Beck J, *et al.* (2017): Striatal fast-spiking interneurons selectively modulate circuit output and are required for habitual behavior. *Elife*. 6: 1–26.
34. Wang X, Gallegos DA, Pogorelov VM, O'Hare JK, Calakos N, Wetsel WC, West AE (2018): Parvalbumin interneurons of the mouse nucleus accumbens are required for amphetamine-induced locomotor sensitization and conditioned place preference. *Neuropsychopharmacology*. 43: 953–963.
35. Yu J, Yan Y, Li K-L, Wang Y, Huang YH, Urban NN, *et al.* (2017): Nucleus accumbens feedforward inhibition circuit promotes cocaine self-administration. *Proc Natl Acad Sci*. 201707822.
36. Robbins TW (2002): The 5-choice serial reaction time task: Behavioural pharmacology and functional neurochemistry. *Psychopharmacology (Berl)*. 163: 362–380.
37. Madisen L, Zwingman TA, Sunkin SM, Oh SW, Zariwala HA, Gu H, *et al.* (2010): A robust and high-throughput Cre reporting and characterization system for the whole mouse brain. *Nat Neurosci*. 13: 133–140.
38. Rothwell PE, Hayton SJ, Sun GL, Fuccillo M V., Lim BK, Malenka RC (2015): Input- and output-specific regulation of serial order performance by corticostriatal circuits. *Neuron*. 88: 345–356.
39. Bari A, Dalley JW, Robbins TW (2008): The application of the 5-choice serial reaction time task for the assessment of visual attentional processes and impulse control in rats. *Nat Protoc*. 3: 759–767.
40. Grissom NM, Herdt CT, Desilets J, Lidsky-Everson J, Reyes TM (2015): Dissociable deficits of executive function caused by gestational adversity are linked to specific transcriptional changes in the prefrontal cortex. *Neuropsychopharmacology*. 40: 1353–1363.
41. Krueger DD, Osterweil EK, Chen SP, Tye LD, Mark F, Huganir RL, *et al.* (2011): Cognitive dysfunction and prefrontal synaptic abnormalities in a mouse model of fragile X syndrome. *Proc Natl Acad Sci*. 108: 2587–2592.
42. Saunders A, Johnson CA, Sabatini BL (2012): Novel recombinant adeno-associated viruses for Cre activated and inactivated transgene expression in neurons. *Front Neural Circuits*. 6: 1–10.
43. Grimm D, Lee JS, Wang L, Desai T, Akache B, Storm TA, Kay MA (2008): In vitro and in vivo gene therapy vector evolution via multispecies interbreeding and retargeting of adeno-associated viruses. *J Virol*. 82: 5887–5911.
44. Lerner TN, Shilyansky C, Davidson TJ, Evans KE, Beier KT, Zalocusky KA, *et al.* (2015): Intact-brain analyses reveal distinct information carried by SNc dopamine subcircuits. *Cell*. 162: 635–647.
45. Hung LW, Neuner S, Polepalli JS, Beier KT, Wright M, Walsh JJ, *et al.* (2017): Gating of social reward by oxytocin in the ventral tegmental area. 1411: 1406–1411.
46. Saunders A, Macosko E, Wysoker A, Goldman M, Krienen F, Bien E, *et al.* (2018): A single-cell atlas of cell types, states, and other transcriptional patterns from nine regions of the adult mouse brain. *bioRxiv*. . doi: 10.1101/299081.
47. Muñoz-Manchado AB, Bengtsson Gonzales C, Zeisel A, Munguba H, Bekkouche B, Skene NG, *et al.* (2018): Diversity of interneurons in the dorsal striatum revealed by single-cell RNA sequencing and PatchSeq. *Cell Rep*. 24: 2179–2190.e7.
48. Fenno LE, Mattis J, Ramakrishnan C, Hyun M, Lee SY, He M, *et al.* (2014): Targeting cells with single

vectors using multiple-feature Boolean logic. *Nat Methods*. 11: 763–772.
49. Kawaguchi Y (1993): Physiological, morphological, and histochemical characterization of three classes of interneurons in rat neostriatum. *J Neurosci*. 13: 4908–23.
50. Cui G, Jun SB, Jin X, Pham MD, Vogel SS, Lovinger DM, Costa RM (2013): Concurrent activation of striatal direct and indirect pathways during action initiation. *Nature*. 494: 238–242.
51. Gunaydin LA, Grosenick L, Finkelstein JC, Kauvar I V., Fenno LE, Adhikari A, *et al.* (2014): Natural neural projection dynamics underlying social behavior. *Cell*. 157: 1535–1551.
52. Dana H, Sun Y, Mohar B, Hulse B, Hasseman JP (2018): High-performance GFP-based calcium indicators for imaging activity in neuronal populations and microcompartments. *bioRxiv*. . doi: 10.1101/434589.
53. Klapoetke NC, Murata Y, Kim SS, Pulver SR, Birdsey-Benson A, Cho YK, *et al.* (2014): Independent optical excitation of distinct neural populations. *Nat Methods*. 11: 338–346.
54. Armbruster BN, Li X, Pausch MH, Herlitze S, Roth BL (2007): Evolving the lock to fit the key to create a family of G protein-coupled receptors potently activated by an inert ligand. *Proc Natl Acad Sci*. 104: 5163–5168.
55. Luk KC, Sadikot AF (2001): GABA promotes survival but not proliferation of parvalbumin-immunoreactive interneurons in rodent neostriatum: An in vivo study with stereology. *Neuroscience*. 104: 93–103.
56. Kita H, Kosaka T, Heizmann CW (1990): Parvalbumin-immunoreactive neurons in the rat neostriatum: a light and electron microscopic study. *Brain Res*. 536: 1–15.
57. Berke JD, Okatan M, Skurski J, Eichenbaum H (2004): Oscillatory entrainment of striatal neurons in freely moving rats. *Neuron*. 43: 883–896.
58. Choi K, Holly E, Davatolhagh MF, Beier KT, Fuccillo M V. (2018): Integrated anatomical and physiological mapping of striatal afferent projections. *Eur J Neurosci*. 1–14.
59. Klug JR, Engelhardt MD, Cadman CN, Li H, Smith JB, Ayala S, *et al.* (2018): Differential inputs to striatal cholinergic and parvalbumin interneurons imply functional distinctions. *Elife*. 7: e35657.
60. Bennet B, Bolam J (1994): Synaptic input and output of neurons in the neostriatum. *Neuroscience*. 62: 707–719.
61. Christakou A, Robbins TW, Everitt BJ (2001): Functional disconnection of a prefrontal cortical-dorsal striatal system disrupts choice reaction time performance: Implications for attentional function. *Behav Neurosci*. 115: 812–825.
62. White MG, Panicker M, Mu C, Carter AM, Roberts BM, Dharmasri PA, Mathur BN (2018): Anterior cingulate cortex input to the claustrum Is required for top-down action control. *Cell Rep*. 22: 84–95.
63. Winters BD, Kruger JM, Huang X, Gallaher ZR, Ishikawa M, Czaja K, *et al.* (2012): Cannabinoid receptor 1-expressing neurons in the nucleus accumbens. *Proc Natl Acad Sci*. 109: E2717–E2725.
64. Jupp B, Caprioli D, Dalley JW (2013): Highly impulsive rats: modelling an endophenotype to determine the neurobiological, genetic and environmental mechanisms of addiction. *Dis Model Mech*. 6: 302–311.
65. Marín O (2012): Interneuron dysfunction in psychiatric disorders. *Nat Rev Neurosci*. 13: 107–20.
66. Selimbeyoglu A, Kim CK, Inoue M, Lee SY, Hong ASO, Kauvar I, *et al.* (2017): Modulation of prefrontal cortex excitation/inhibition balance rescues social behavior in CNTNAP2-deficient mice. *Sci Transl Med*. 9. doi: 10.1126/scitranslmed.aah6733.
67. Kalanithi PS a, Zheng W, Kataoka Y, DiFiglia M, Grantz H, Saper CB, *et al.* (2005): Altered parvalbumin-positive neuron distribution in basal ganglia of individuals with Tourette syndrome. *Proc Natl Acad Sci U S A*. 102: 13307–12.
68. Burguière E, Monteiro P, Feng G, Graybiel AM (2013): Optogenetic stimulation of lateral orbitofronto-striatal pathway suppresses compulsive behaviors. *Science (80-)*. 340: 1243–1246.
69. Gernert M, Hamann M, Bennay M, Löscher W, Richter A, Loscher W, Richter A (2000): Deficit of striatal parvalbumin-reactive GABAergic interneurons and decreased basal ganglia output in a genetic rodent model of idiopathic paroxysmal dystonia. *J Neurosci*. 20: 7052–7058.
70. Rapanelli M, Frick LR, Xu M, Groman SM, Jindachomthong K, Tamamaki N, *et al.* (2017): Targeted interneuron depletion in the dorsal striatum produces autism-like behavioral abnormalities in male but not female mice. *Biol Psychiatry*. 82: 194–203.
71. Xu M, Li L, Pittenger C (2016): Ablation of fast-spiking interneurons in the dorsal striatum, recapitulating abnormalities seen post-mortem in Tourette syndrome, produces anxiety and elevated grooming. *Neuroscience*. 324: 321–329.
72. Voon V, Irvine MA, Derbyshire K, Worbe Y, Lange I, Abbott S, *et al.* (2014): Measuring “waiting” impulsivity in substance addictions and binge eating disorder in a novel analogue of rodent serial reaction time task. *Biol Psychiatry*. 75: 148–155.